CHAPTER IV
RESULTS AND DISCUSSION

4.1 Characterization of Precursors

4.1.1 Characterization of Silatrane Precursor

Silatrane was synthesized by the Oxide One Pot Synthesis (OOPS) process. The product obtained was a white powder and the structure was shown in fig 4.1. The TGA result of silatrane (fig. 4.2) showed one major transitions of the weight loss at 400°C with 22.36 % ash yield corresponding to $Si((OCH_2CH_2)_3N)_2H_2$. The % ceramic yield of the product was higher than the theoretical ceramic yield (18 %) due to the incomplete combustion of the product which can be confirmed by the final ash was dark in color. Moreover, FTIR spectrum as seen in fig. 4.3 shows the characterization peak of silatrane at 785 to 729 and 579 cm^{-1} corresponding to Si-O-C and Si←--N, respectively.
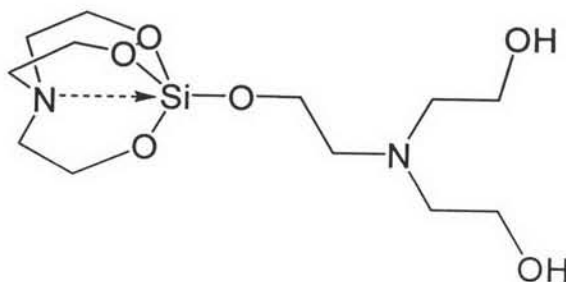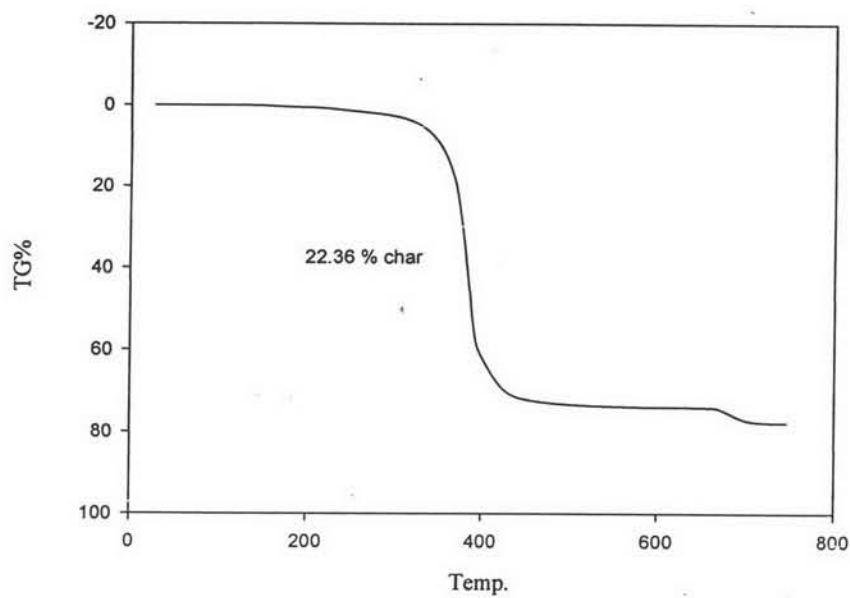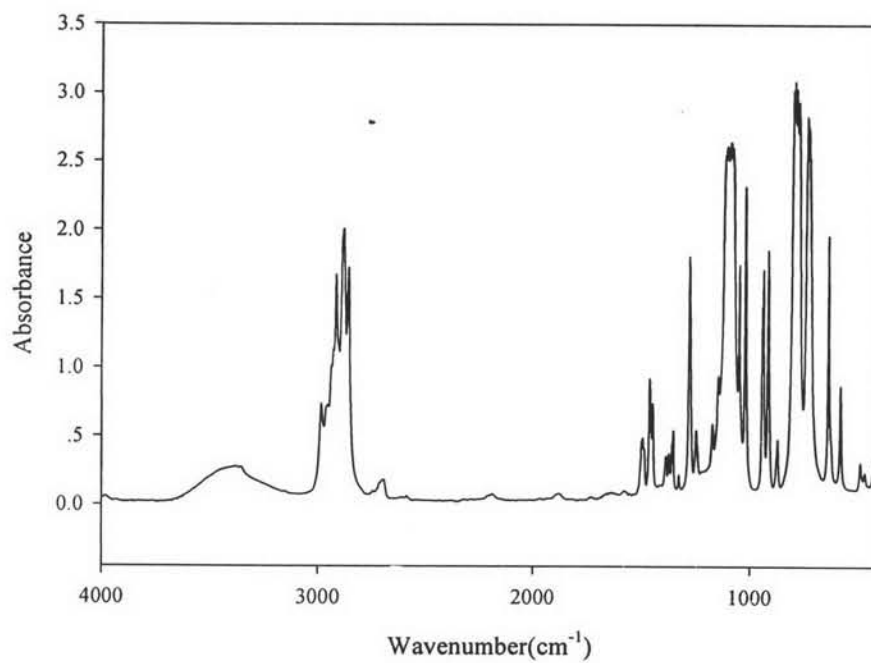

Figure 4.1 The structure of Silatrane.
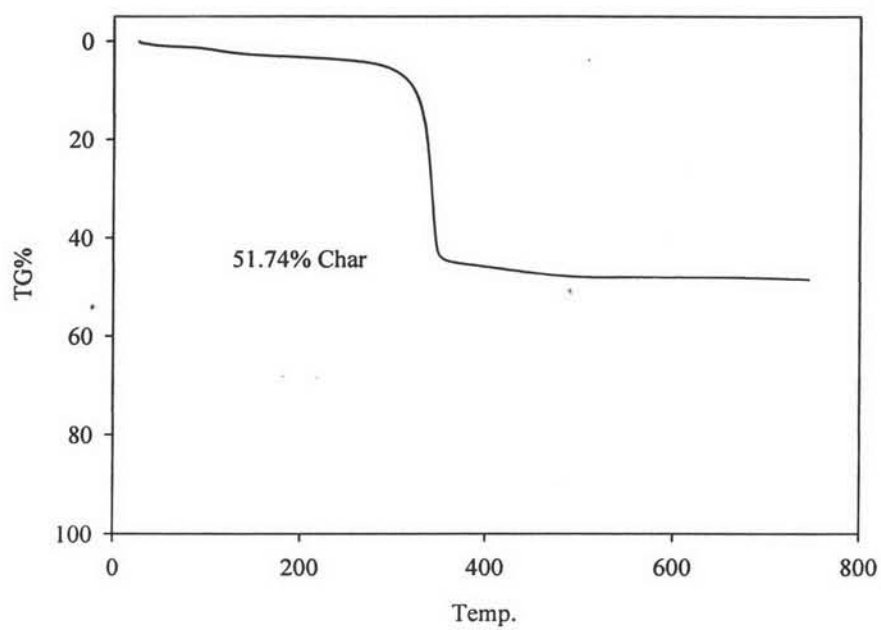
Figure 4.2 TGA result of Silatrane Precursor.

Figure 4.3 FTIR result of Silatrane Precursor.
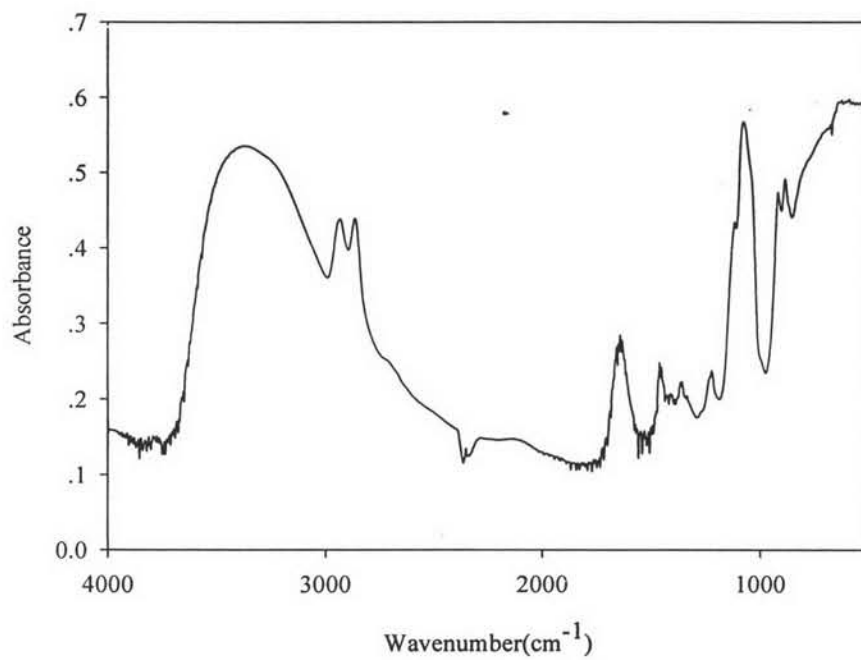
4.1.2 Characterization of Titanium Glycolate Precursor

Titanium glycolate precursor was also synthesized via the OOPS process using inexpensive and widely available TiO_2 as staring material, ethylene glycol and triethylenetetramine, TETA, as a base. Since water was a by-product of the reaction, it must be removed from the system to push the reaction forward, as illustrated in equation.

$$TiO_2 \quad + \quad HO\!\!\diagdown\!\!\diagup\!\!OH \quad \xrightarrow[\text{200°C / under } N_2]{\text{+TETA / -H}_2\text{0}} \quad $$
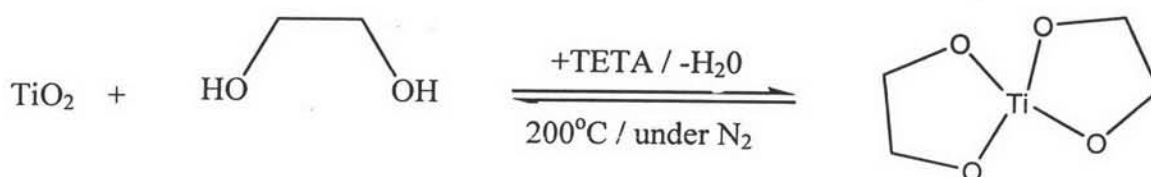
TGA analysis of titanium glycolate was carried out in nitrogen atmosphere and the result is shown in fig. 4.4. The first weight loss around 310-350°C corresponds to organic ligand decomposition of remaining organic residue. The final ash yield is 51.7% which is higher than the theoretical ceramic yield, 47.56%, based on the final ceramic product of TiO_2. FTIR spectrum and assignment of titanium glycolate are shown in fig. 4.5. The band around 2855-2927 cm^{-1} is assigned to the C-H stretching of glycolate ligand. Three bands at 1130, 1080 and 1042 cm^{-1} can be assigned to C-O-Ti, characteristics of glycolate ligand linked to titanium. The presence of the band at 619 cm^{-1} is assigned to Ti-O stretching.
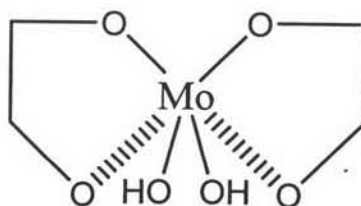
Figure 4.4 TGA result of Titanium Glycolate Precursor.

Figure 4.5 FTIR result of Titanium Glycolate Precursor.

4.1.3 Characterization of Molybdenum Glycolate Precursor

The molybdenum glycolate was synthesized by the OOPS process to obtain white solid and the structure is shown in fig 4.6. TGA result showed five mass loss transitions corresponding to: 150°C (H_2O molecule absorbed by molybdenum glycolate molecule, also confirmed by FTIR), 210°C (H_2O molecule generated from decomposition of molybdenum glycolate), 350°C (glycolate ligand of molybdenum glycolate molecule), 430°C (the other ligand of molybdenum glycolate molecule) and 720°C (carbon residues) with 43.9% ash yield, as shown in fig. 4.7, corresponding to $Mo(OH)_2(O(CH_2)_2O)_2$ having 56.7% theoretical yield. When taking off the first mass loss of water absorbed by the product, the ash yield having 58.9% became closer to the theoretical yield. For FTIR result (fig. 4.8) the bands observed at 946 and 533 cm^{-1} are assigned to the Mo-O-C and Mo-O stretching, respectively.

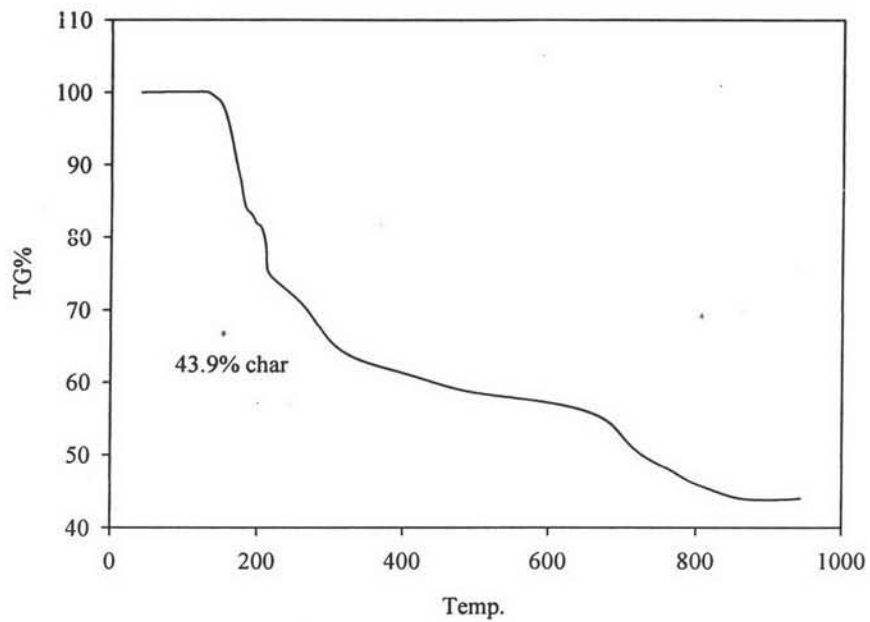**Figure 4.6** The structure of Molybdenum Glycolate Precursor.

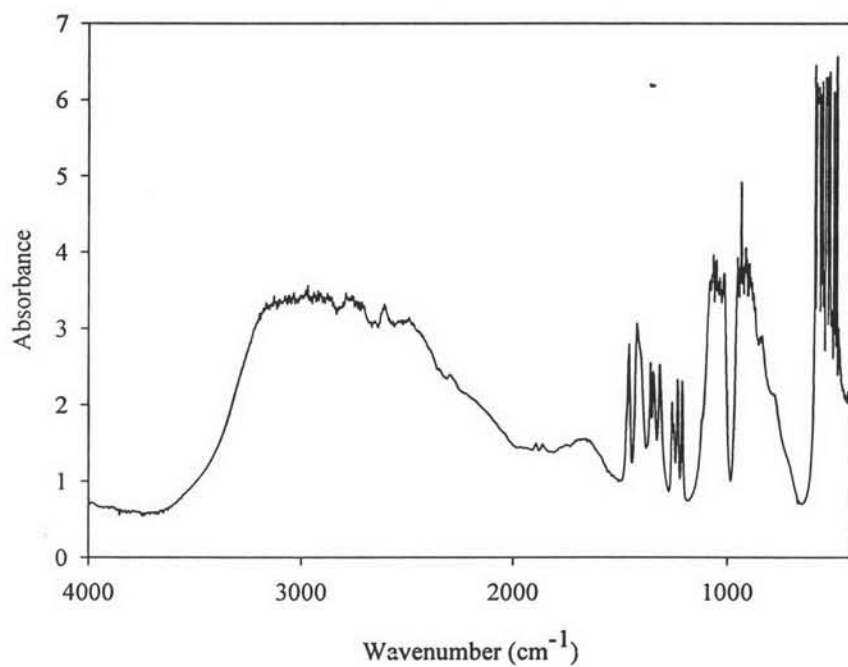**Figure 4.7** TGA result of Molybdenum Glycolate Precursor.

Figure 4.8 FTIR result of Molybdenum Glycolate Precursor.

4.2 Characterization of Ti-MCM-41 and Mo-MCM-41 Catalysts

Ti-MCM-41 and Mo-MCM-41 were synthesized via the sol-gel process to obtain white powder. DRUV used to determine the presence of framework and extra-framework titanium species shows tetrahedral coordinated species at λ = 200-230 nm, see fig. 4.9. They are in good agreement with Chatterjee, *et al.* in 2002 and Marchese, *et al.* in 1997. When %Ti increased, the DRUV peak was broader and showed a shoulder at λ = 280 nm, referring to partially polymerized Ti species, as discussed by Thanabodeekij, *et al.* in 2005. It was also reported that the absorption band from DRUV pattern (fig. 4.10) of Mo-MCM-41 from 230-280 nm was assigned to Mo (T_d) and the band from 270-330 nm was assigned to Mo (O_h) by Williams, *et al.* in 1991. It was also found in this work. Moreover, the intensity of the band increased with increasing Mo content, and none of the samples exhibited absorption at wavelengths longer than 350 nm, representing molybdenum oxide. That means, molybdenum glycolate have no aggregated molybdenum oxide species, but rather only highly dispersed Mo-oxides. (Shinya Higashimoto *et al.*, 2005). The calcined products at various %Ti and %Mo contents showed a well-resolved pattern of hexagonal mesostructure, as shown in fig. 4.11 and 4.12, respectively. In the figures, XRD spectra give only hk0 reflections and no reflections at diffraction angles larger than 6 degree 2θ were observed. The three-peak positions of 100, 110 and 200 reflections are from long-range structural order of hexagonal arrays. In addition, the considerably good intensity still maintains even % loaded Ti increases. The discovered tendency is similar to the results in the reference (Thanabodeekij, N *et al.*, 2005). The main reason for this remarkable result probably comes from our extraordinary precursors having highly pure and moisture stable properties. However, at high %Mo, the XRD patterns showed lower crystallinity, as indicated by the lower intensity of 100 reflections peak, the smaller and less isolated 110 and 200 reflection peaks. In MCM-41 structure, there are OH groups (Si–OH), and these silanols may act as functional groups to react with other molecules. In the present work, the dispersion of molybdenum and formation of Mo oxide species are related to the silanol groups of MCM-41 (J. Leyrer, *et al.* 1986) by possibly attacking of Mo

to a nearby strained Si–O–Si bond or silanol to generate a Si–O–Mo bridge (Morey M.S., *et al.*, 2000). The formation of Si–O–Mo bonds in the treated samples may increase the strained extent of siloxane bonds, which are susceptible to hydrolysis within the wall of MCM-41 (M.V. Landau, *et al.*, 1999).

Nitrogen physisorption probes the textural properties of materials, such as, surface area, pore size and pore volume. The BET surface area, pore size and pore volume of Ti-MCM-41 and Mo-MCM-41 are summarized in Table 4.1. The pore size of Mo-MCM-41 was observed to increase from 3.351 to 5.059 nm as increasing the amount of Mo loaded. An increase in the unit cell size parameter was also noted on the incorporation of Mo ions into meso-frameworks. This phenomenon is coincided with the data from previous analyses (Shinya Higashimoto *et al.*, 2005). The result corresponds to a decrease in pore wall thickness of the crystallite sample and indicates that the titanium substituted MCM-41 could be crystallized without decreasing mesoporous size via our normal synthesis process (Thanabodeekij, N *et al.*, 2005). Surprisingly, the amount of Ti loading onto MCM-41 via the sol-gel process did not affect the BET surface area and the pore size. The same results were also observed at higher amount of molybdenum dispersed into MCM-41. It was also noticed by Gamal, Shafei and Mokhtar in 1994 that the blocking of those pores with sizes in the range of narrow mesoporous was responsible for this result. The higher probability of the presence of adjacent hydroxyls in narrow pores was thus behind in surface area characteristics.
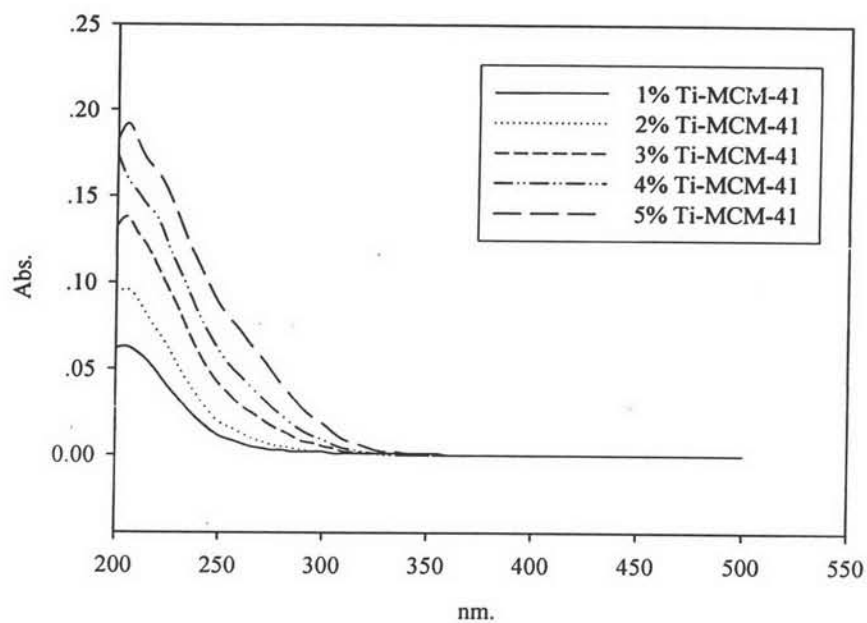
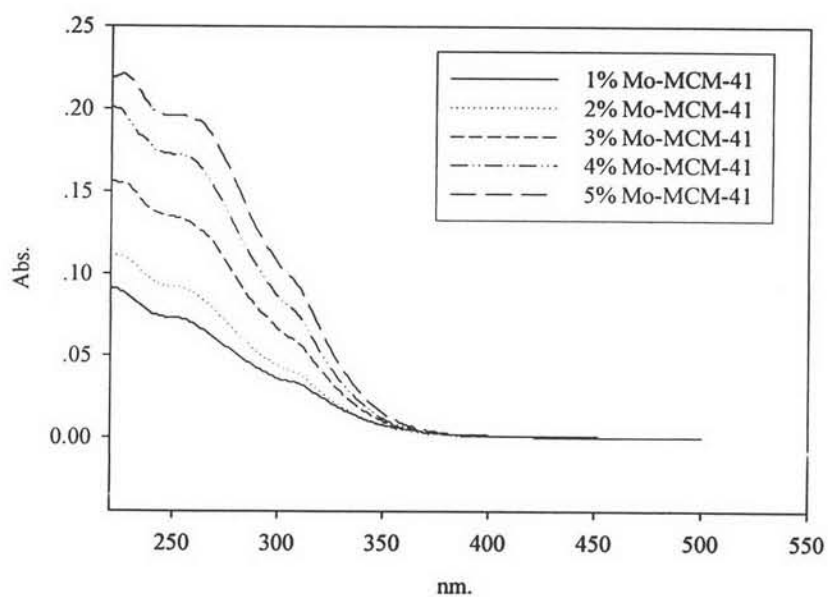**Figure 4.9** DRUV results of various Ti-MCM-41 catalysts.

Figure 4.10 DRUV results of various Mo-MCM-41 catalysts.
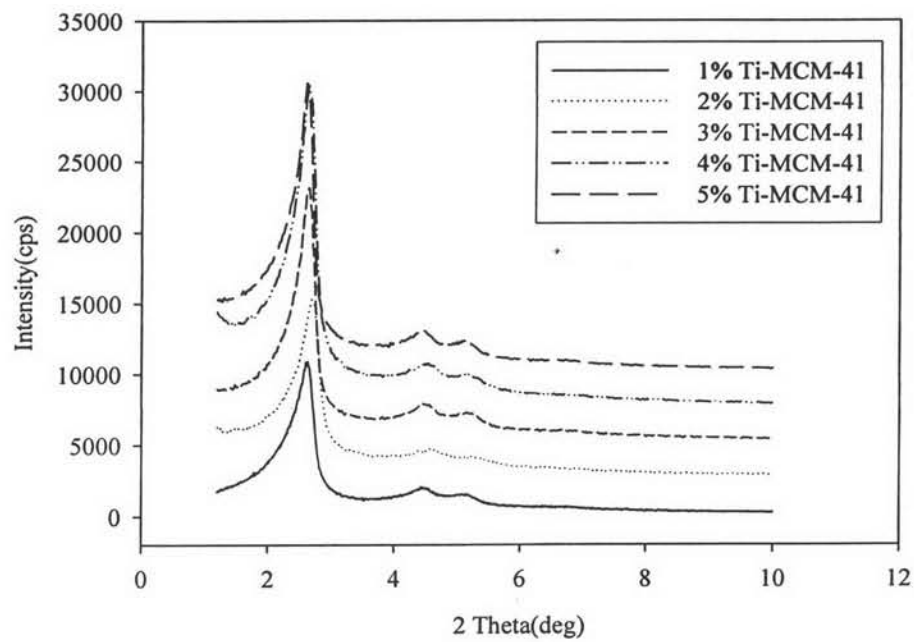
Figure 4.11 XRD results of various Ti-MCM-41 catalysts.
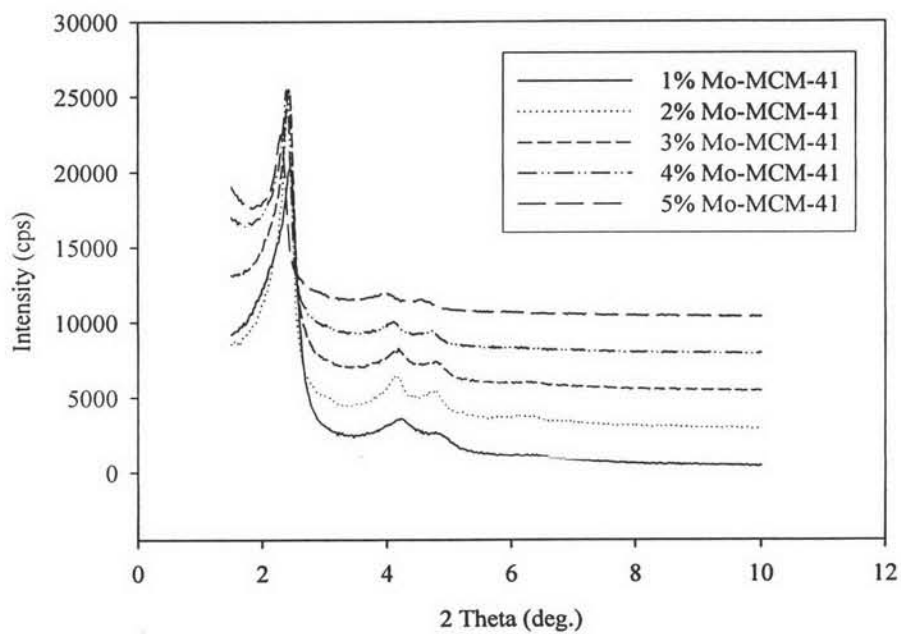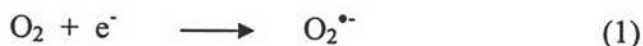

Figure 4.12 XRD results of Mo-MCM-41 catalysts.

Table 4.1 The BET analysis of Ti-MCM-41 and Mo-MCM-41 synthesized at different Ti loadings and Mo dispersions.
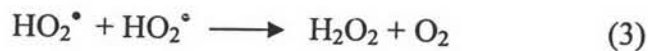
| Catalyst	BET Surface Area (m^2/g)	Pore Volume (cc/g)	Average Pore Size (nm)
1% Ti-MCM-41	1299	0.8265	2.545
2% Ti-MCM-41	1333	0.8570	2.571
3% Ti-MCM-41	1276	0.7457	2.338
4% Ti-MCM-41	1451	0.9060	2.498
5% Ti-MCM-41	1187	0.8200	2.764
1% Mo-MCM-41	1376	1.150	3.351
2% Mo-MCM-41	1133	1.043	3.683
3% Mo-MCM-41	959.5	0.9542	3.978
4% Mo-MCM-41	983.4	1.123	4.569
5% Mo-MCM-41	738.6	0.9341	5.059

4.3 Photocatalytic Oxidation Process

4.3.1 Effects of pH and H_2O_2 on Photocatalytic Oxidation Process

Reaction time needed for degradation and decolorization depends mainly upon the concentration and stability of the solution. Almost all dyes molecules are consisted of atomic systems having abundant π-electrons, which are responsible for color. Structural or electron distribution changes possibly induced by protons lead to color change. The results of various pHs in degradation and decolorization of the dye from TOC and UV-Vis (fig. 4.13 and 4.14, respectively) showed the highest efficiency at pH 3. This could be explained that in acidic solution the azo groups and the SO_3^- groups connected to the central naphtal are protonated. Thus, most hydroxyl radicals probably add to the azo groups although some also attacks the aromatic rings (K. Dajka *et al.* 2003). Moreover, the oxygen molecules in the air also influence on photocatalytic oxidation, as demonstrated in equations below (C. Tang and V. Chen 2004). Under acidic conditions, the steps for H_2O_2 production from oxygen are possible (Houas A, *et al.* 2001).

$$O_2 + e^- \longrightarrow O_2^{\bullet-} \qquad (1)$$

$$O_2^{\bullet-} + H^+ \longrightarrow HO_2^{\bullet} \qquad (2)$$

$$HO_2^\bullet + HO_2^\bullet \longrightarrow H_2O_2 + O_2 \qquad (3)$$

The degradation is enhanced by the presence of H_2O_2 that can generate hydroxyl radicals during the photocatalytic reaction (Mariana Neamtu *et al.* 2002). Degradation of organic compounds on oxidative degradation by free radical attack, particularly by hydroxyl radical, is a far more powerful oxidizing agent among all commonly known oxidants. Hydrogen peroxide activated with UV light decomposes into hydroxyl radicals. The results of various concentrations of H_2O_2 (10, 20 and 30 mmol) in fig. 4.15 and 4.16 showed that the highest activity was obtained at 30 mmol of H_2O_2. Thus, it can be concluded that a good and suitable condition for further study is at pH 3 with 30 mmol of H_2O_2 in 40 mg/L of reactive black 5 dye solution.
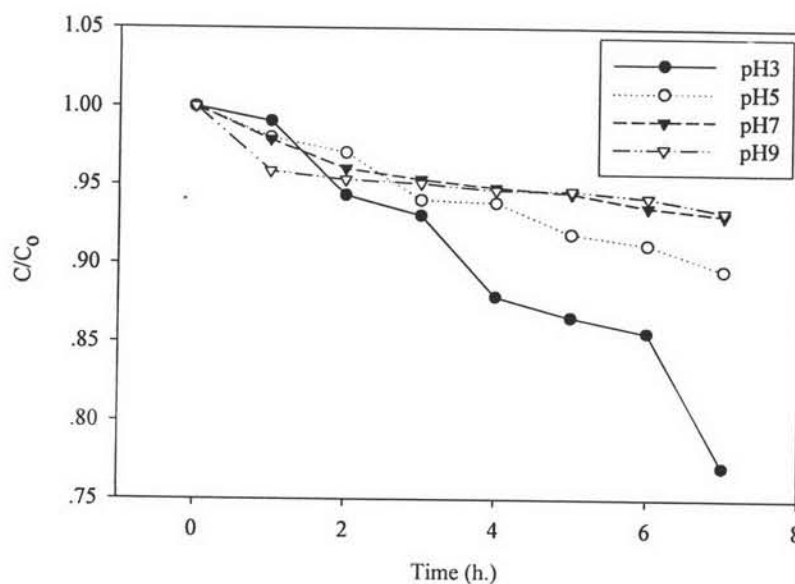
Figure 4.13 TOC results of various pHs (3, 5, 7 and 9).

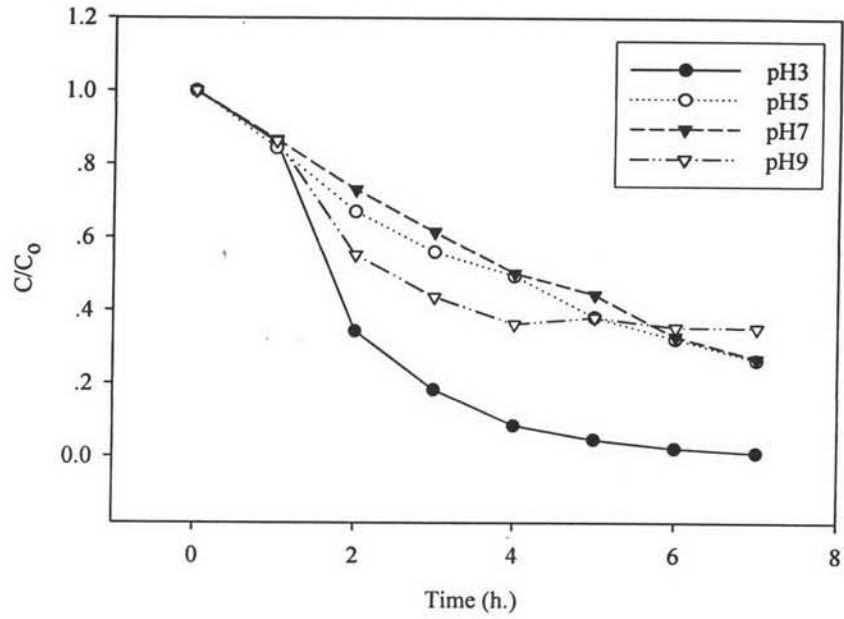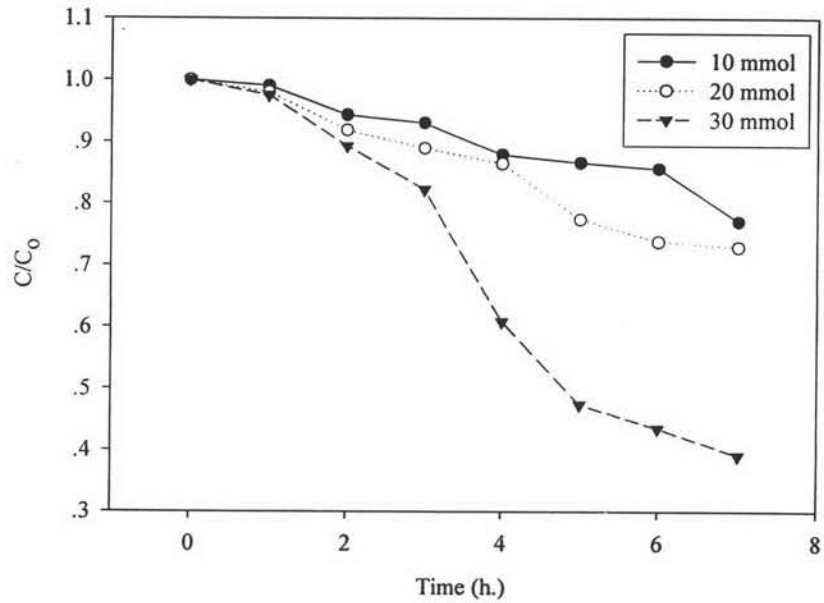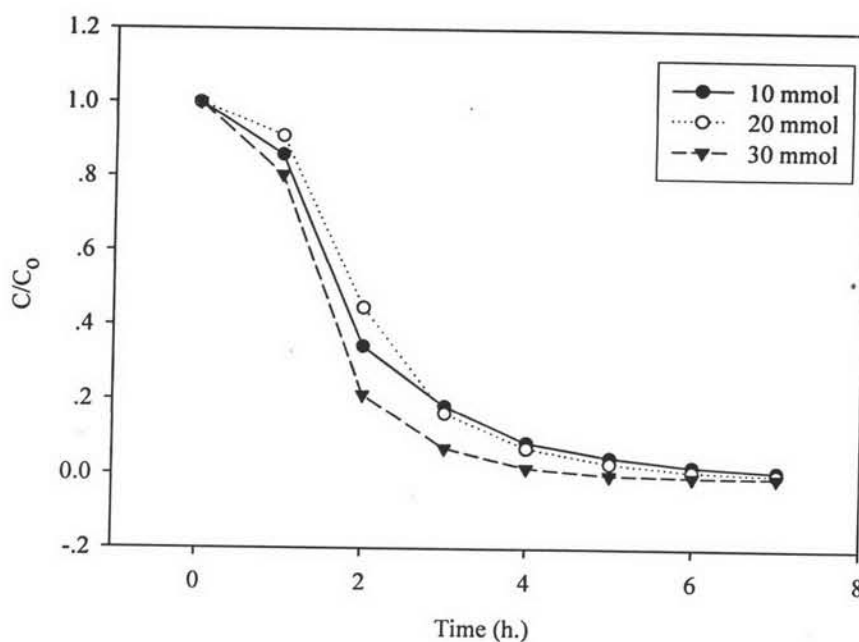**Figure 4.14** UV-Vis results of various pHs (3, 5, 7 and 9).
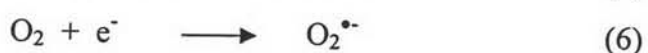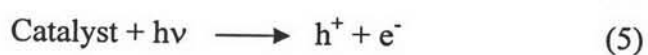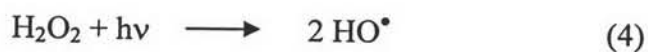

Figure 4.15 TOC results of various concentrations of H_2O_2 (10 mmol, 20 mmol and 30 mmol).

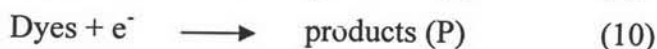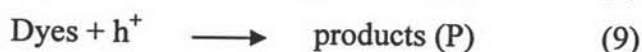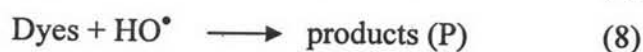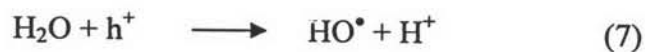**Figure 4.16** UV-Vis results of various concentrations of H_2O_2 (10 mmol, 20 mmol and 30 mmol).

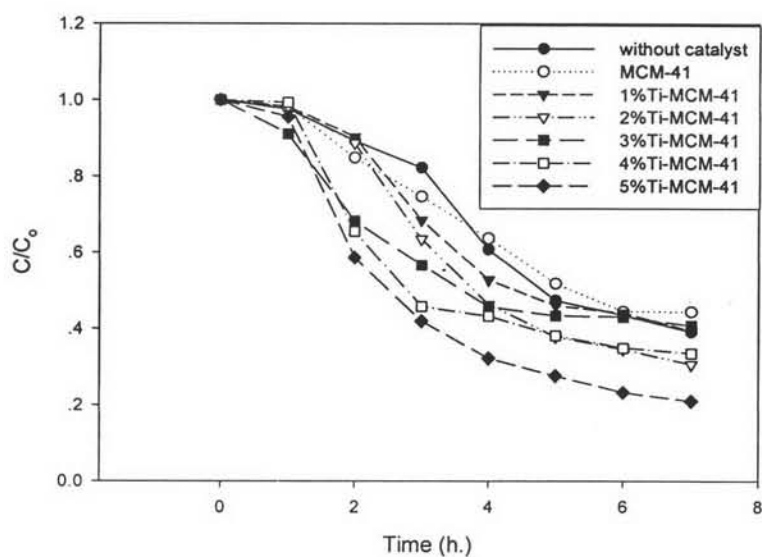### 4.3.2 Photocatalytic Oxidation Process of Ti-MCM-41 and Mo-MCM-41 Catalysts

A group of scientists did propose that besides equations 1, 2 and 3, under at least eigth more reactions were probably taken place; hydrogen peroxide photolysis (4), catalyst photolysis (5), formation of superoxide radical anion (6), formation of hydroxyl radical (7), generating highly reactive HO• radicals giving primary products (8), direct oxidation by reaction with holes (9), direct electron transfer from catalyst to dye molecule (10) and oxidation of primary products (P) with HO• to mineral compounds (11) (Mariana Neamtu 2002, C. Tang and V. Chen 2004 and M. Saquib and M. Muneer 2002):

$$H_2O_2 + h\nu \longrightarrow 2\,HO^{\bullet} \qquad (4)$$

$$Catalyst + h\nu \longrightarrow h^+ + e^- \qquad (5)$$

$$O_2 + e^- \longrightarrow O_2^{\bullet-} \qquad (6)$$

$$H_2O + h^+ \longrightarrow HO^\bullet + H^+ \qquad (7)$$

$$Dyes + HO^\bullet \longrightarrow products\ (P) \qquad (8)$$

$$Dyes + h^+ \longrightarrow products\ (P) \qquad (9)$$

$$Dyes + e^- \longrightarrow products\ (P) \qquad (10)$$

$$P + HO^\bullet \longrightarrow final\ products \qquad (11)$$
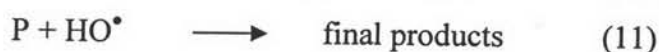
The initial step between hydrogen peroxide and catalyst, consisting of Ti-oxide or Mo-oxide, under UVA light was proposed to involve the generation of $HO^\bullet$, h^+ and e^-, leading to the formation of superoxide radical, hydroxyl radical, primary products and final products, as shown in equations (4)-(11). Photoexcitation of semiconductor leads to the formation of electron hole pair, which can eventually bring about redox reaction from organic substrates dissolved in water. Alternatively, the electron in the conducting band can be picked up by the adsorbed dye molecules, leading to the formation of dye radical anion, and subsequent reaction of the radical anion can lead to degradation of the dye (M. Saquib and M. Muneer 2002). When photocatalytic degradation of reactive black 5 was performed at various amounts of Ti and Mo loaded MCM-41 (1, 2, 3, 4 and 5%) at pH 3 and 30 mmol H_2O_2, the results demonstrated that the more Ti and Mo was loaded onto MCM-41, the better degradation was observed, according to fig. 4.17 to fig. 4.21. In acidic solution a higher adsorption of dye on the catalyst leads to a faster decrease of the dye concentration (Abdelkahhar Aguedach et al. 2005). The results show that the degradation and decoloration of reactive black 5 are enhanced by the presence of Ti and Mo due to the holes (h^+) and electron (e^-) generated during the photochemical reaction. As can be seen in fig. 4.23, the results of 5%Mo-MCM-41 show better efficiency of degrading reactive black 5 dyes than 5%Ti -MCM-41. It can be explained that band-gap irradiation of oxide semiconductor affects the generation of hold (h^+) and photoexcited electron (e^-)(Shicheng Zhang et al., 1997), meaning that the band gap of Mo-MCM-41 should be narrower than that of Ti-MCM-41. Therefore, the closer band gap leads to easier production of hold (h^+) and photoexcited electron (e^-). The band gap determines the wavelength of light that can be absorbed. Delocalized bands are necessary to keep the electron-hole pair from

recombining after their formation. Band edges determine the possible surface redox reactions. The band edge positions are affected by the charge transfer energy from the metal to oxygen, the local coordination and symmetry of the metal. Local coordination can changes the band gap depending on the co-valency of the ion to oxygen (H.W. Eng and P.M. Woodward). According to fig. 4.19 and 4.22, the degradation of reactive black 5 dyes confirmed using UV-Vis spectroscopy showed that when the reaction time increased, the peak height around 580 nm, which is the λ_{max} of reactive black 5, decreased. The degradation was complete at the aging time around 3 h although the TOC result showed the presence of organic compounds, converted from the dye molecule.
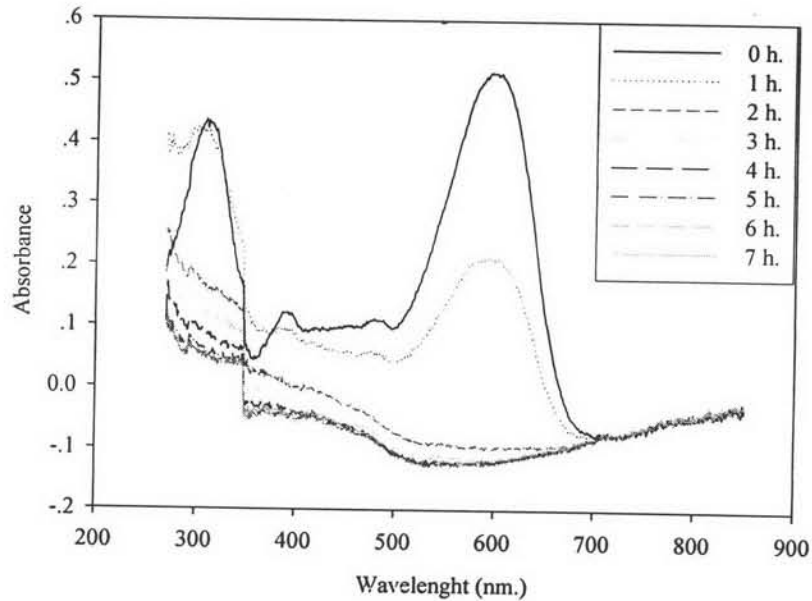

Figure 4.17 TOC results of photocatalytic oxidation process by various amounts of Ti loaded on MCM-41 (1, 2, 3, 4 and 5%).
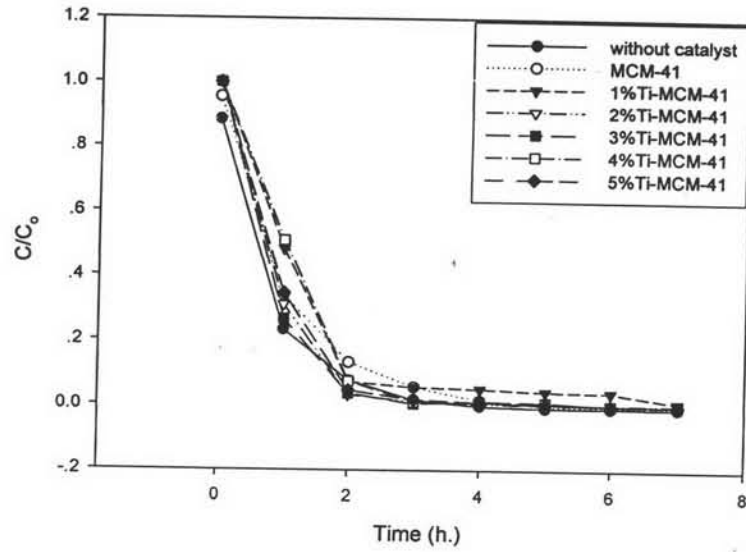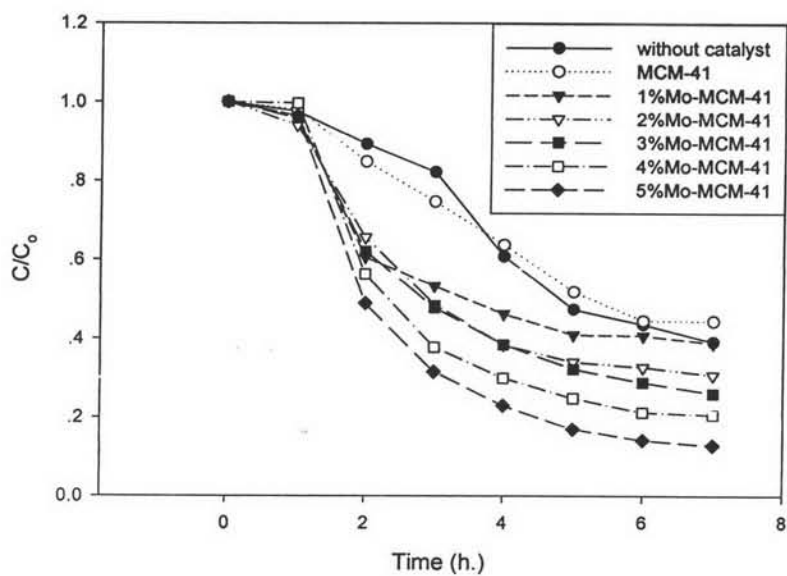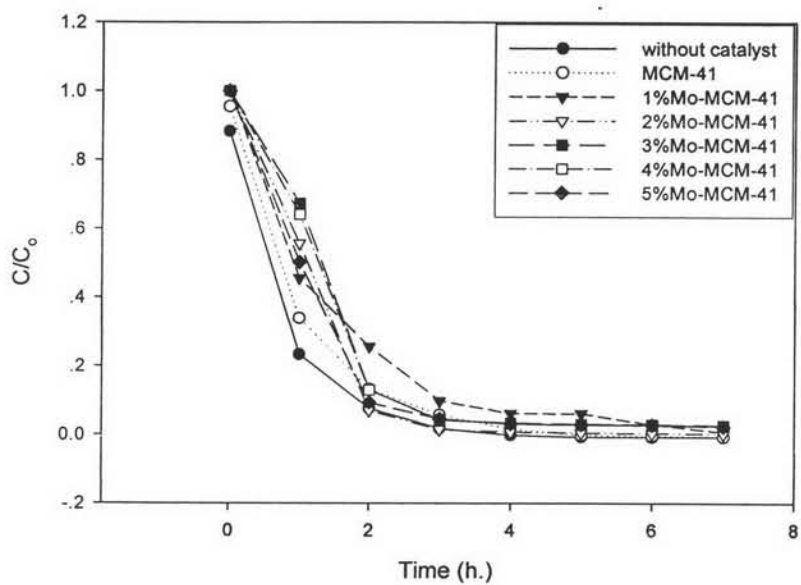
Figure 4.18 UV-Vis results of photocatalytic oxidation process by various amounts of Ti loaded on MCM-41 (1, 2, 3, 4 and 5%).
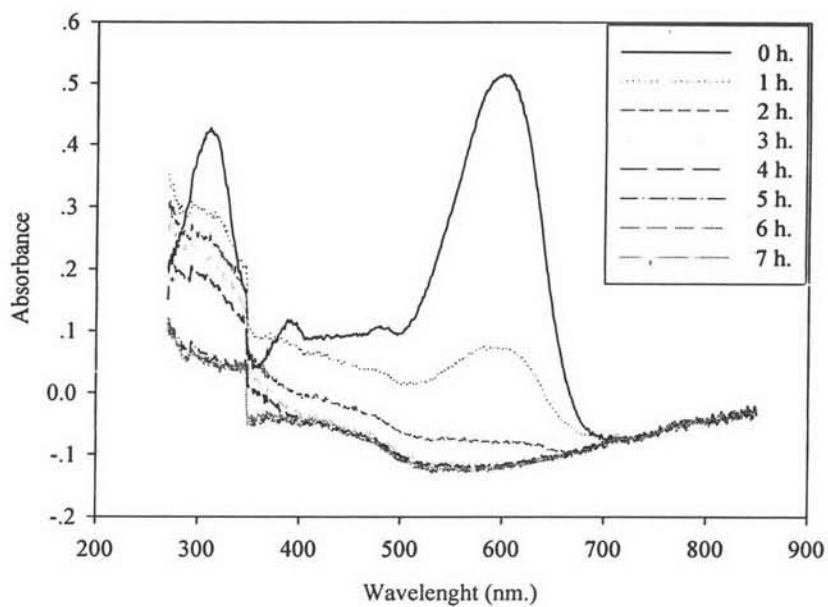

Figure 4.19 UV-Vis spectra of photocatalytic oxidation process using 5%Ti-MCM-41
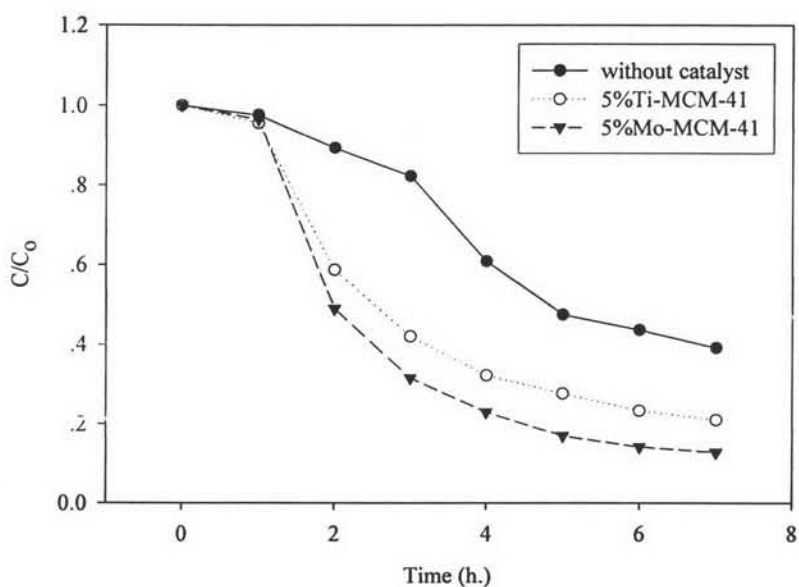
Figure 4.20 TOC results of photocatalytic oxidation process by various amounts of Mo loaded on MCM-41 (1, 2, 3, 4 and 5%).

Figure 4.21 UV-Vis results of photocatalytic oxidation process by various amounts of Mo loaded on MCM-41 (1, 2, 3, 4 and 5%).

Figure 4.22 UV-Vis spectra of photocatalytic oxidation process using 5%Mo-MCM-41.

Figure 4.23 TOC results of photocatalytic oxidation process using without catalyst, 5%Ti-MCM-41 and 5%Mo-MCM-41.